Engineering Solid Mechanics 12 (2024) 93-102

Contents lists available at GrowingScience

Engineering Solid Mechanics

homepage: www.GrowingScience.com/esm

Experimental analysis on microstructure, mechanical properties, and corrosion behavior of TIG welded AISI 444 ferritic stainless steels

Prashant Kumar Pandey[a], Rajeev Rathi[b*], Mahipal Singh[a] and Jagesvar Verma[c]

[a]*School of Mechanical Engineering, Lovely Professional University, India*
[b]*Department of Mechanical Engineering, National Institute of Technology, Kurukshetra, India*
[c]*Department of Mechanical and Manufacturing Engineering, National Institute of Advanced Manufacturing Technology, Ranchi, Jharkhand, India*

ARTICLEINFO

Article history:
Received 10 March 2023
Accepted 4 July 2023
Available online
4 July 2023

Keywords:
Ferritic Stainless Steel
Tungsten Inert Gas Welding
Mechanical Properties
Microstructure
Corrosion Behavior

ABSTRACT

This research aims to evaluate the potential of using AISI 444 (ferritic stainless steel) in critical weld joints. For the last several years serious efforts have been made in the area of welding stainless steel. While the problems associated with the performance of welded joints of ferritic stainless steel (FSS) are still there. In the current work, an effort has been made to create sound weld joints while also examining the microstructural, mechanical, and corrosion-resistance characteristics of the weldment. To evaluate the weldments' corrosion resistance, modified destructive and non-destructive tests were conducted in an aggressive environment. The research findings revealed that the joint's ferrite content was balanced. Weld showed higher hardness than the base metal. The tensile properties were examined experimentally, and the tensile test proved that these steel welds are stronger than those of the base metal. This effect might also be felt in the heat-affected zone (HAZ), which is the area right close to the fusion zone. In comparison to the sulfuric acid solution, the HCL solution showed stronger effects.

1. Introduction

Various grades of stainless steel mainly comprising austenitic stainless steel, ferritic stainless steel, martensitic stainless steel, and duplex stainless steel are available and used for different industrial applications (Verma & Taiwade, 2017). Out of these available grades of stainless steel, ferritic stainless steel (FSS) covers a significant area mainly including chemical and petrochemical industries where stainless steel is being utilized (Tavares *et al.*, 2008). In the past decade, there has been a substantial increase in interest in the development of FSS weld joints, and in connection therewith, many attempts have been made to guarantee a great life for these welded connections. Due to its superior mechanical qualities and improved weldability, 444 FSS is well known for its wide range of applications, which are expanding quickly (Arivarasu *et al.*, 2015). Ferritic stainless steel is utilized where hardness, wear resistance, or increased strength is required since the hardenability of steel improves with carbon concentration. Instead of high strength, several grades of FSS are chosen for wear resistance, and parts are frequently heat-treated to achieve desirable qualities. Chromium-containing ferritic stainless steels have body-centered cubic (bcc) crystal structures (Prashar & Vasudev, 2021).

Although 444 FSS is ferromagnetic and has adequate ductility, its high-temperature mechanical qualities are not as good as those of austenitic stainless steel. At low temperatures, the toughness is also unnatural (Li *et al.*, 2019). Because they contain less chromium and nickel, ferritic stainless steels often have superior technical qualities than austenitic grades (Saeidi *et al.*, 2016). Whether the ferritic stainless steel is joined with a comparable or different weld substance, is fairly common. Both metal combinations are employed in a variety of applications, and these joints are highly sought after by businesses in

* Corresponding author.
E-mail addresses: rathi.415@gmail.com (R. Rathi)

ISSN 2291-8752 (Online) - ISSN 2291-8744 (Print)

doi: 10.5267/j.esm.2023.6.001

the pulp and paper, shipbuilding, nuclear power, and petrochemical industries, among other sectors (Prashar and Vasudev, 2022). In contrast to austenitic stainless steels, which are simple to weld, FSS is challenging to weld due to the issue of coarse grains in the weld zone and heat-affected zone of fusion weld (Qu *et al.*, 2013). Sensitization, which happens as a result of the development of either chromium carbides or nitrides at grain boundaries, is the main issue with FSS. Around the carbides, where they originate, a chromium-depleted zone results, making the steel vulnerable to intergranular corrosion (Vasudev *et al.*, 2020). The suitable welding methods to join FSS plates with a thickness of around 10 mm are manual metal arc (MMA) welding, gas tungsten arc welding (GTAW), gas metal arc welding (GMAW), hybrid laser-TIG welding, etc (Singh *et al.*, 2023; Dong *et al.*, 2022).

Literature reveals that FSS welds are nearly flawless and fully penetrated. These welds can offer satisfactory performance with reasonable cost savings, based on both technical and economic considerations (Sathiya *et al.*, 2007). Another study performed experiments and found that to ensure better fatigue life of the weld joints, intermittent welds should be preferred over welds with long continuous weld runs. The selection of a class of weld is very crucial as it directly affects the allowable stress range for fatigue (Zhang *et al.*, 2018). The location of the heat sources has an impact on the weld's integrity in terms of its geometry, microstructure, micro-segregation, and mechanical qualities. When the heat source is placed away from the contact, the weld microstructure's homogeneity is reduced, which causes noticeable hardness differences. The production of martensitic structures is caused by the heat source driving the cooling rate at the weld metal contact (Vasudev *et al.*, 2021). The addition of nitrogen to an argon-based shielding gas during FSS gas tungsten arc welding allows for the development of equiaxed grains, which raise the microhardness of the weld metal as the nitrogen dissolves into the weld pool. The hardness of the weld metal also greatly rises as a result of microstructure refinement (Ambade *et al.*, 2019). In a study, it was observed that the heat-affected zone (HAZ) of FSS exhibits substantial grain growth relative to the base metal in the partially-melted zone (Silva *et al.*, 2008). Regardless of the welding energy used, the presence of fine needle-like precipitates is observed known as Laves phase. Fine-dispersed precipitation is another effect of the weld heat cycle in the HAZ (Delgado *et al.*, 2016). At the ferrite grain boundaries, chi and sigma phase precipitation have also been found in some locations (Mallaiah *et al.*, 2012).

The literature undoubtedly states that there is relatively less information available so far regarding the welding of FSS 444 grade plates with any of the fusion welding processes and the effect on microstructure, mechanical properties, and corrosion resistance of these weld joints. The inspiration for the current work came from this. In the present study, the preparation of weld joints of a 3mm thick FSS 444 grade plate has been done by using the GTAW technique and then the characterization of microstructure behavior and mechanical properties has been investigated.

This paper aims to evaluate the potential of AISI 444 FSS in critical weld joints. In the current work, an attempt has been made to find out the numerous factors that have a substantial impact on FSS performance. Weld joints of FSS (AISI 444) using TIG have been developed with optimum process parameters. However, the study of the mechanical properties, microstructure, and corrosion behavior of 444 FSS weldments with the TIG process are scarce.

2. Materials and methods

For the current study AISI444 grade, FSS plates are selected with a thickness of 3 mm. The material was received in the form of plates with sizes of 300 × 300 × 3 mm, composed mainly of a bcc phase, and exhibits metallurgical traits that are comparable to Fe-Cr alloys that include enough Cr (more than roughly 12%) to stay outside the γ -loop and prevent the formation of an undue volume of the brittle phase. It is a typical constituent of FSS. The chemical composition of the selected material is shown in Table 1.

Table 1. Chemical Composition of AISI 444 (wt%)

Elements	%C	%Mn	%S	%P	%Si	%Ni	%Cr	%Mo	%N	Fe
AISI 444	0.015	≤ 1.00	≤ 0.03	≤ 0.04	0.54	≤ 1.00	17.5	1.75-2.5	≤ 0.012	Balance

The tungsten inert gas welding process has been selected to prepare the weld joint due to its immense and versatile use. Argon is used as a shielding gas, however, AWS A5.9 ER 308L has been used as a filler metal. The selected wire size of this filler metal was 1.2 mm dia. The typical chemical composition of this filler metal is presented in Table 2.

Table 2. Chemical Composition of AWS A5.9 ER 308L (wt%)

C	Mn	Mo	S	Si	Cr	Ni	Fe
0.024	1.65	0.02	0.002	0.42	20.10	10.33	Bal.

The weld joint design (Fig. 1) has been selected, the joint for a particular thickness of a material is to be welded by the TIG Process with gas at a flow rate of 15 l/min and argon is used as an inert gas.

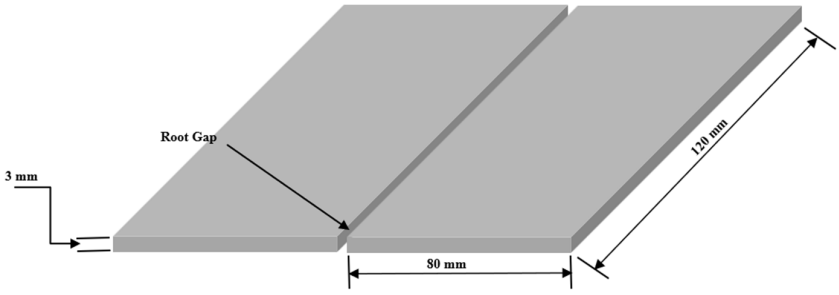

Fig. 1. Weld Geometry

The main process parameters of the TIG process are; welding current, welding voltage, welding speed, and shielding gas pressure. An exhaustive study was carried out to find out the recommended welding parameters of the TIG process for welding FSS, and after identifying the suitable parameters pilot (sample) weld joints were developed (Kalpana, Rao, *et al.*, 2017).

3. Experimental Procedure

3.1 Sample preparation

While preparing the weld joint it was ensured to have the heat input was as low as possible. Pilot weld joints were prepared starting with a low heat input (90 A, 24V) and then further welding parameters were used and characterization of weld bead geometry was done. The problems which were experienced in the process of obtaining a sound weld joint are incomplete penetration, excessive reinforcement, uneven weld bead, excessive penetration, arc spatter, etc. Instead of these defects, it was also found that the root gap (1.2 mm) selected for the pilot weld joints, decreases simultaneously as the welding progress due to the expansion of the plates at the root face by thermal expansion. Because of this, the gap between the plates decreases which further hinders the penetration of filler wire leading to insufficient melting at the root of the joint. Post-sample weld joints preparation, the weld joint characterizations were done and a final weld joint was prepared as shown in Fig. 2.

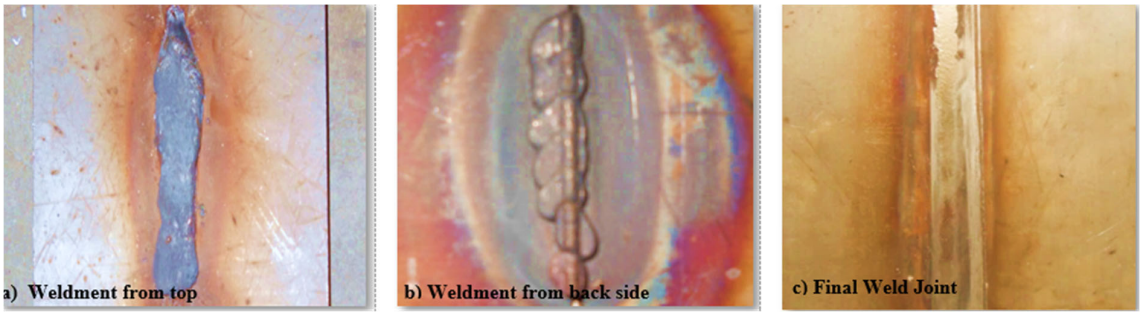

Fig. 2. Weld Appearance

With help of the welding process parameter optimization and characterization of the pilot weld joints, the optimum parameters were found (Table 3) and the final weld joint (Fig. 2) was developed accordingly for further studies.

Table 3. Optimized Welding Process Parameters for GTAW process

Welding Current	Welding Voltage	Welding Travel Speed	Shielding Gas flow rate (l/min)
108 A	24 V	12 cm/min	15

To ensure that the developed weld joint is defect-free or not, Ultrasonic Testing was performed and some flaws were found at the starting and end of the weld bead. To obtain better test results the weld material from these locations was removed in the transverse direction of the weld.

3.2 Mechanical Testing

Before the preparation of test specimens for mechanical testing, visual inspections, and X-ray radiographic tests were conducted for the welded joints to detect any surface or subsurface defects like porosity, cracks, voids, etc. inside the weldment (Kalpana, Srinivasa Rao, *et al.*, 2017). The test specimens were prepared with the help of a wire-cut EDM process to ensure minimum microstructural changes as compared to other conventional metal cutting/machining processes and then the tests were carried out.

3.2.1 Hardness Test

For the hardness test, the same specimen (figure 3) was used which was prepared for the microstructure study. The hardness test of the weld, heat-affected zone, and base metal of the weld joint was carried out by the Vickers microhardness test method, while the indentations were taken at a load of 100 gms. The hardness was taken at different closest locations to ensure the best results. The data obtained from the hardness test is used to study the hardness behavior in different regions along the weld joint.

Fig. 3. Specimen for Microstructure and Hardness Test

3.2.2 Tensile Test

The tensile test was done on a hydraulically operated dynamic universal testing machine as per ASTM E8 M-04. The ultimate tensile load, stress-strain curve, and failure mode characteristics were recorded for each specimen (Kumar *et al.*, 2022). SEM was then used to analyze the fractured faces of the tensile-tested specimens. Considering the thickness (small) of the plate used for the current study sub-sized tensile specimens were prepared. The dimension of the specimen is confirmed in Fig. 4.

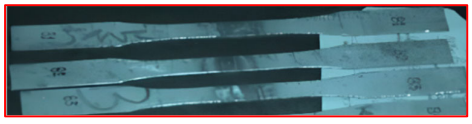

Fig. 4. The specimen for the tensile test as ASTM E8 standard

3.2.3 Impact Test

A Charpy impact test was conducted using a 300 J machine. The loaded notched specimen is subjected to plastic deformation at the notch region. The Charpy impact test calculates the amount of energy expended when a notched sample is hammered by a swinging impactor while merely resting on both ends (Arivarasu *et al.*, 2015). When the specimen can no longer absorb energy, normal stress begins to develop at the base of the notch, and fracture occurs. The difference between the sample's drop height before and after the fracture serves as a measure of the impact energy that the sample has absorbed. Through ultrasonic cleaning, the fractographic inspection is carried out. To investigate the impact toughness of weld metal (WM) transverse test samples were created as per the American Society for Testing and Materials (ASTM) - E23 standards as shown in the Fig. 5.

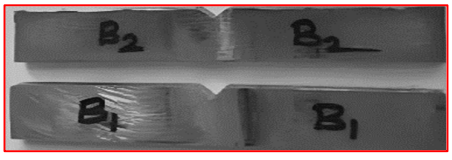

Fig. 5. Impact test specimen

3.2.4 Metallographic and Microstructural Characterization

Specimen (refer to Fig. 3) for metallographic examination was collected from the transverse section across the center line of the weld joint and polished with various grades of emery papers (120,220,300,400,800 and 1000) from coarse to fine respectively. Then the specimen was polished on a polishing wheel. The polished specimen was etched in a solution of glycerine (5 cc), acetic acid (10 cc), nitric acid (10 cc), and hydrochloric acid (15cc) by dipping them into the etchants for 60-80 seconds followed by washing with a stream of water and drying the specimen. The microstructural study of the weld was carried out using an optical microscope. A scanning electron microscope equipped with an energy-dispersive x-ray spectroscopy instrument (SEM/EDX, FEI XL30) was applied to gather higher magnifications of the microstructure and chemical composition over the interface region and selected locations in both the base metal and weld metal (Saeheaw, 2023). SEM analysis was carried out to find out the fracture behavior of tensile-tested specimens of base metal and weld metal. Samples for this analysis were obtained from the tensile-tested specimens by cutting them, adjacent to the fractured portion. To find the chemical composition of different alloying elements at a particular location in the weld metal, an EDAX analysis was carried out. Sample preparation for the SEM analysis of weld metal was used for this analysis also.

3.2.5 Corrosion Studies

Weight loss tests

Rectangular samples having a cross-sectional area of 0.60 cm^2 were cut for weight loss testing. To suspend the sample in the tank and connect the string, a hole with a diameter of 4 mm was drilled at one end of the sample. Before stringing the sample, it was polished with emery paper up to a 1200 grade, then rinsed in distilled water to get rid of any dirt or oils that

had built up on the surface. Polished and pre-weighed samples were subjected to 0.1 M hydrochloric acid and 0.1 M sulphuric acid (H_2SO_4). At room temperature, all of the experiments were run. At three-day intervals, weight loss measurements were taken throughout the 60-day experiment on weight loss. Micrometers per year were used to calculate the corrosion rate. Two trials were performed in each instance, and the outcomes differed within the bounds of allowable experiment error. Before moving on to the next round of tests, the electrolytes were adjusted. The corrosion rates of the samples were calculated using the formula (Vasudev *et al.*, 2022).

$Rcorr = 10^4$ ML/ (ρ.A.t)
where Rcorr = µm/y
ML = mass loss, g, and A = samples exposed surface area, cm^2.
t = exposure time, yr
ρ = density of samples, g/cm^3
Modified immersion test:
To evaluate the pitting behavior in a very aggressive environment, the modified immersion test was also carried out. A sample measuring 15 mm × 10 mm × 3 mm was immersed.

4. Results and Discussion

4.1 Microstructural analysis

The microstructures of the weld metal (WM), fusion line, heat affected zone (HAZ), and base metal (BM have been studied to find out the behavior of the grain growth and its structure at different locations along the weld joint. Micrographs (Fig. 6) have been taken at different magnifications with the help of an optical microscope to ensure a better understanding of the microstructure. In weld metal, columnar grains have been observed. The precipitation of carbide and other alloying elements has been observed at the grain boundary, while the dark spot (Fig. 5a) shows the inclusions of foreign elements during welding. The microstructure at the fusion line shows the epitaxial solidification near the fusion boundary. At the fusion line, the columnar grains have been observed which further transform into dendrites due to the higher cooling rate during solidification. Due to this higher cooling rate fine dendritic structure has been observed in the HAZ. The white regions in HAZ show the presence of ferrite. The microstructure of base metal depicts the presence of predominate ferrite.

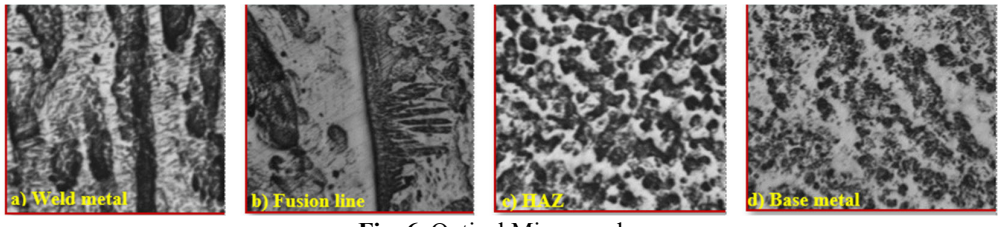

Fig. 6. Optical Micrographs

4.2 Microhardness

The hardness test has been carried out to find the Vicker's hardness Number (HV) at different locations in the weld metal (WM), heat affected zone (HAZ) as well as in base metal (BM) at different locations. The hardness distributions in these regions are plotted and shown in Fig. 7.

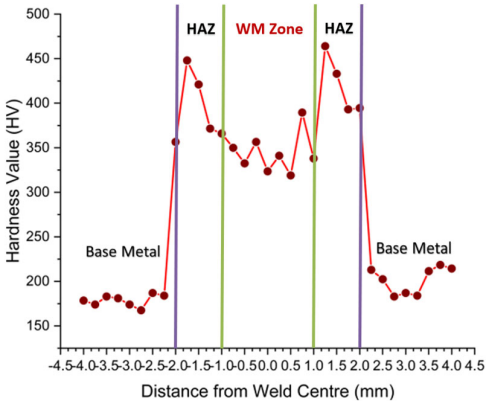

Fig.7. Hardness Distributions in Weld Metal**,** HAZ, and Base Metal

It is observed that the average hardness in HAZ is more than in weld metal and base metal. It is probably due to martensite transformation in HAZ adjacent to weld which may be experienced in the weld thermal cycle also. Work hardening may be

another cause of this variation in hardness. The effectiveness of martensite transformation can be reduced significantly by heating (annealing) during welding.

4.3 Tensile Test

The ultimate tensile strength, yield strength, and percent elongation of the base metal as well as the weld joint have all been determined using the tensile test. Three tensile specimens were tested using a universal testing machine and stress-strain curves (Fig. 8) for these three specimens have been plotted. It has been observed that all three specimens prepared for the tensile test failed from the base metal region.

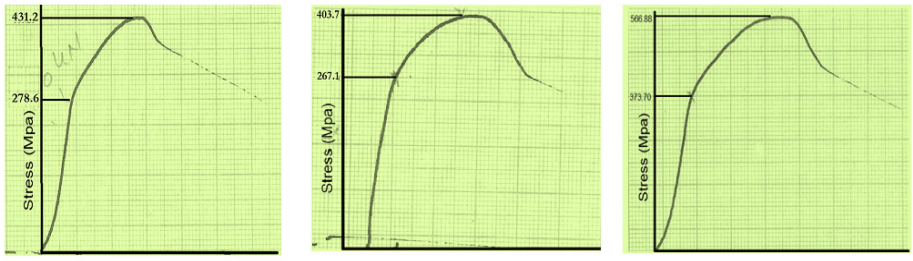

Fig. 8. Stress-Strain Curve of Tensile Test Specimens

Based on the data obtained, using the stress-strain curves and with further calculations, vital mechanical properties have been obtained (Table 4) and further summarized in Fig. 9. It can be concluded from the tensile test that weld metal is stronger as compared to base metal since all the specimens failed from the base metal region. The weld metal becomes stronger since the strength of steel mainly depends on heat flow and its rate. Heat flow from weld metal towards base metal happens to follow a quenching-like effect. It should also be noted here that alloy steels undergo heat treatment processes to increase ductility at the expense of ultimate strength, depending on the composition. The welded metal from these steels is stronger and harder than the base metal it is surrounded by. The heat-affected zone, which is the region next to the fusion zone, may also experience this impact. In this situation, post-weld heat treatment is frequently performed to regain some ductility.

Table 4. Tensile Test Results

S.No.	UTS (Mpa)	Yield Stress (Mpa)	% Elongation	Location of Failure
1	431.2	278.6	16.67%	BM
2	403.7	267.1	15.2%	BM
3	566.88	373.70	18.33%	BM

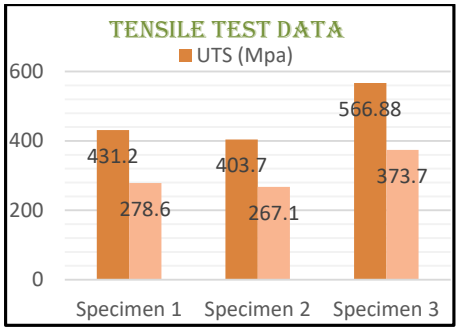

Fig. 9. Tensile Properties of Specimens

4.4 Impact Toughness

The average impact toughness for the samples taken was nearly 30 J to cause a fracture in the received condition using Charpy-V notch reduced size samples. However, using an unnotched sample the impact toughness reached a value over 100 J which indicates that AISI 444 steel has a high sensitivity to notches.

4.5 Fractograph

As the specimens were fractured from the base metal, therefore analysis of any of the specimens will be enough to characterize the morphology of base metal fracture mode. The micrograph (Fig. 10) shows that the fracture surface is in the

form of dimples which is evidence of the occurrence of ductile fracture in the base metal, while the small holes/voids indicate the availability of more strain before fracture. The presence of fine dimples on the fracture surface is evidence of high strength and ductility. The fractography shows relatively minor size dimples surrounded by coarse dimples and a small quantity of tearing ridge. These dimples typically develop as a result of the material's micropore combination during plastic deformation. Fractures began at the center of the specimens and then extends towards the outer surface by a shear separation.

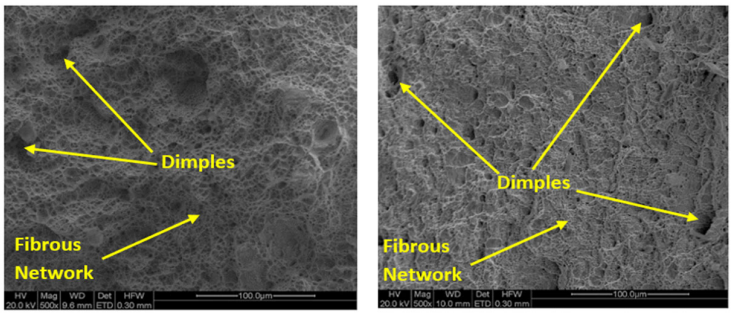

Fig. 10. Scanning Electron Micrographs of Fracture Surface of Base Metal

4.6 EDAX Analysis of Weld Metal

EDAX analysis of weld metal has been performed to determine the composition of alloying elements at a particular location in the weld metal. Chromium, nickel, and manganese peaks are present, according to the EDX examination. From figure 11, it can be observed that the weight percentages for the element Cr have a value of 15.76%, Si has a value of 0.81%, Mn has a value of 2.25%, Fe has a value of 70.13%, Ni has a value of 3.18%. When comparing the material's nominal chemical composition before and after welding, it can be seen that the weight percentage of chromium (Cr) has reduced while the weight percentage of iron (Fe) has increased post-welding.

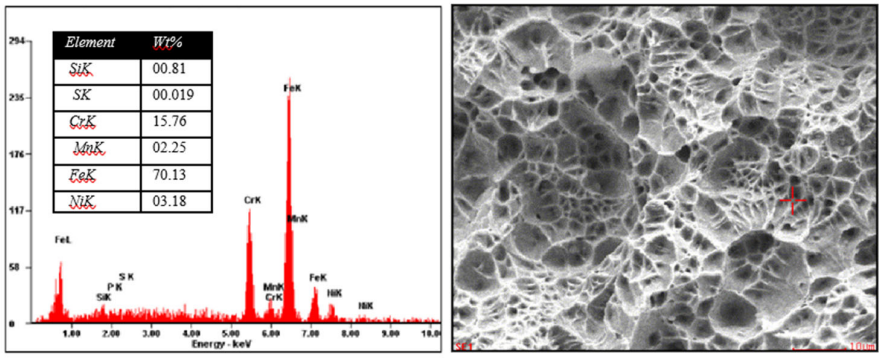

Fig. 11. Elemental Distribution of Alloying Element in Weld

4.7 Corrosion studies

60 days of weight loss measurements in 0.1 M solutions of sulphuric acid, 0.1 M hydrochloric acid, and 0.1 M sulphuric acid with 3.5% sodium chloride were used to study the corrosion behavior of the alloy. It was noted that the solutions changed to a dark green color when the alloy was submerged in the 0.1 M concentration of all the used solutions. On the first cycle of the test, there was a noticeable increase in the alloy's weight loss, but no further appreciable change was seen until the test was through. According to Table 5, Alloy 444 showed the greatest weight loss in terms of corrosion rate in the HCL solution than the sulphuric acid solution.

Table 5. The corrosion rate in different corrosive solutions

Media	Corrosion Rate
H_2SO_4	2.25×10^3
HCL	4.20×10^2

For the modified immersion test sample were dipped in boiling 42% $MgCl_2$ solution and maintained the temperature of 100 ˚C, for 80 h. A heavy pit was discovered in the sample following the test. On the phase border, there were several cracks visible in the SEM micrograph (Fig. 12). In every instance, the deep grooving and grain dropping were evident. This test

resulted in the degradation of components and indicated the sample's vulnerability in this environment for 80 hours. 0.13 g of mass was lost throughout the weight decrease.

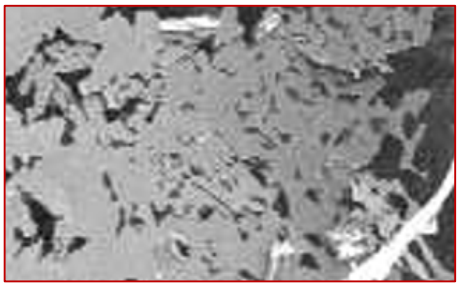

Fig. 12. SEM image of the sample in modified immersion test

5. Conclusion, limitation and future research direction

The FSS weld joints produced by the TIG technique showed sound joints. The microstructure of the weld was comprised of the ferritic matrix with intragranular martensite transformation that can further be reduced by heating (annealing) up to a great extent. The highest hardness was measured in HAZ followed by WM, while the lowest was in BM, principally because martensitic transformation is a possibility. Heat treatment procedures after welding may help the weld joints regain their ductility and hence improve their mechanical properties. The highest tensile strength was found in weld metal since all tensile test specimens failed from the base metal. The presence of ductile fracture in the base metal is confirmed by scanning electron microscopy (SEM), and the impact toughness test findings employing Charpy V notched reduced-size samples show that the material AISI 444 has significant notch sensitivity. The EDAX analysis confirms that the elemental composition of the welded samples has changed. The weight loss test reveals that 444 loses weight significantly more quickly in the HCL solution than in the sulphuric acid solution. The modified immersion test identified the materials' vulnerability to corrosive environments that destroyed materials.

References

Ambade, S. P., Sharma, A., Patil, A. P., & Puri, Y. M. (2021). Effect of welding processes and heat input on corrosion behaviour of Ferritic stainless steel 409M. *Materials Today: Proceedings*, *41*, 1018-1023.

Arivarasu, M., Ramkumar Kasinath, D., & Natarajan, A. (2015). Effect of continuous and pulsed current on the metallurgical and mechanical properties of gas tungsten arc welded AISI 4340 aeronautical and AISI 304 L austenitic stainless steel dissimilar joints. *Materials Research*, *18*, 59-77.

Delgado, A. J., Ambriz, R. R., Cuenca-Álvarez, R., Alatorre, N., & López, F. F. (2016). Heat input effect on the microstructural transformation and mechanical properties in GTAW welds of a 409L ferritic stainless steel. *Revista de Metalurgia*, *52*(2), 68-77.

Dong, Z., Li, Y., Lee, B., Babkin, A., & Chang, Y. (2022). Research status of welding technology of ferritic stainless steel. *The International Journal of Advanced Manufacturing Technology*, 1-27.

Kalpana, J., & Rao, P. (2017). Effect of vibratory welding process on hardness of dissimilar welded joints. *Engineering Solid Mechanics*, *5*(2), 133-138.

Kalpana, J., & Rao, P. (2017). A review on techniques for improving the mechanical properties of fusion welded joints. *Engineering Solid Mechanics*, *5*(4), 213-224.

Kumar, G. S., Ramesh, M., Dinesh, S., Paramasivam, P., & Parthipan, N. (2022). Investigation of the TIG welding process for joining AA6082 alloy using grey relational analysis. *Advances in Materials Science and Engineering*, *2022*.

Li, Y., Du, P. F., Jiang, Z. H., Yao, C. L., Bai, L., Wang, Q., ... & Li, H. B. (2019). Effects of TiC on the microstructure and formation of acicular ferrite in ferritic stainless steel. *International Journal of Minerals, Metallurgy and Materials*, *26*(11), 1385-1395.

Mallaiah, G., Kumar, A., Reddy, P. R., & Reddy, G. M. (2012). Influence of grain refining elements on mechanical properties of AISI 430 ferritic stainless steel weldments–Taguchi approach. *Materials & Design (1980-2015)*, *36*, 443-450.

Prashar, G., & Vasudev, H. (2021). A comprehensive review on sustainable cold spray additive manufacturing: State of the art, challenges and future challenges. *Journal of Cleaner Production*, *310*, 127606.

Prashar, G., & Vasudev, H. (2022). Structure–property correlation of plasma-sprayed Inconel625-Al2O3 bimodal composite coatings for high-temperature oxidation protection. *Journal of Thermal Spray Technology*, *31*(8), 2385-2408.

Qu, H. P., Lang, Y. P., Yao, C. F., Chen, H. T., & Yang, C. Q. (2013). The effect of heat treatment on recrystallized microstructure, precipitation and ductility of hot-rolled Fe–Cr–Al–REM ferritic stainless steel sheets. *Materials Science and Engineering: A*, *562*, 9-16.

Saeheaw, T. (2023). Comparison of different supervised machine learning algorithms for bead geometry prediction in GMAW process. *Engineering Solid Mechanics*, *11*(2), 175-190.

Saeidi, K., Kevetkova, L., Lofaj, F., & Shen, Z. (2016). Novel ferritic stainless steel formed by laser melting from duplex stainless steel powder with advanced mechanical properties and high ductility. *Materials Science and Engineering: A*, *665*, 59-65.

Sathiya, P., Aravindan, S., & Noorul Haq, A. (2007). Effect of friction welding parameters on mechanical and metallurgical properties of ferritic stainless steel. *The International Journal of Advanced Manufacturing Technology*, *31*, 1076-1082.

Silva, C. C., Farias, J. P., Miranda, H. C., Guimaraes, R. F., Menezes, J. W., & Neto, M. A. (2008). Microstructural characterization of the HAZ in AISI 444 ferritic stainless steel welds. *Materials characterization*, *59*(5), 528-533.

Singh, M., Goyat, R., & Panwar, R. (2023). Fundamental pillars for industry 4.0 development: implementation framework and challenges in manufacturing environment. *The TQM Journal*.

Tavares, S. S. M., De Souza, J. A., Herculano, L. F. G., De Abreu, H. F. G., & de Souza Jr, C. M. (2008). Microstructural, magnetic and mechanical property changes in an AISI 444 stainless steel aged in the 560 C to 800 C range. *Materials characterization*, *59*(2), 112-116.

Vasudev, H., Prashar, G., Thakur, L., & Bansal, A. (2021). Electrochemical corrosion behavior and microstructural characterization of HVOF sprayed Inconel-718 coating on gray cast iron. *Journal of Failure Analysis and Prevention*, *21*, 250-260.

Vasudev, H., Thakur, L., Singh, H., & Bansal, A. (2022). Effect of addition of Al2O3 on the high-temperature solid particle erosion behaviour of HVOF sprayed Inconel-718 coatings. *Materials Today Communications*, *30*, 103017.

Verma, J., & Taiwade, R. V. (2017). Effect of welding processes and conditions on the microstructure, mechanical properties and corrosion resistance of duplex stainless steel weldments—A review. *Journal of Manufacturing Processes*, *25*, 134-152.

Zhang, W., Jiang, W., Zhao, X., & Tu, S. T. (2018). Fatigue life of a dissimilar welded joint considering the weld residual stress: Experimental and finite element simulation. *International Journal of Fatigue*, *109*, 182-190.